Korean Chem. Eng. Res., 63(3), 105120 (2025)
https://doi.org/10.9713/kcer.2025.63.3.105120
PISSN 0304-128X, EISSN 2233-9558

Performance and Exergy Analysis of Enhanced Integrated Reverse Multi-Stage Flash and Multi-Effect Evaporator Systems

Emad Ali*,† and Jamel Orfi**

*Chemical Engineering Department, King Saud University, Riyadh,11421, Saudi Arabia
**Mechanical Engineering Department, King Saud University, Riyadh, 11421, Saudi Arabia
(Received 9 September 2024; Received in revised from 23 January 2025; Accepted 23 January 2025)

Abstract – Hybridization of a reversal multistage flash (MSFRV) and multi-effect evaporators (MEE) purification methods was investigated. A waste heat source was employed to drive the hybrid system while the thermal energy of the MSFRV reject brine was utilized as a sensible heat supply to the MEE process. The novelty of the work relied on constructing a sustainable and energy-efficient desalination system. Efficiency was achieved by integrating two desalination technologies to capitalize on their advantages and minimize their deficiencies. Sustainability was sought through leveraging internal energy and utilization of low-grade energy. The boosted hybrid configuration recorded 561%, 91%, and 83% improvement in the recovery ratio, the specific energy consumption, and the gain output ratio compared to the standalone MSFRV. The recovery ratio, normalized heat transfer area, levelized energy consumption, and gain output ratio were found to enhance correspondingly with the feed temperature, and the temperature change across the MEE sensible heat supplier. The best proposed hybrid configurations belonged to the one with booster units that produced additional vapor. The superiority of this structure was not only due to the elevated production rate but also to the efficient utilization of internal energy instead of incurring additional heat exchanger or external cooling water. The exergy analysis indicated that the hybrid system without boosters was the most efficient structure in terms of lowest exergy destruction and highest exergy efficiency. Indeed, it exhibited around 32% less exergy losses and about 17% higher exergy efficiency.

Key words: Water desalination, Reverse multistage flash, Multi-effect evaporator, Hybridization, Waste energy

1. Introduction

Presently, the most challenging mission facing humanity's survival and development is the continuous supply of drinkable water. The dire need for potable water has been rising by 1% since 1980s and it is anticipated that this demand rate will grow to 20–30% by 2050. There are many reasons for this increasing demand, but the evolving world population is the most effective factor as the global population is projected to approach 9.7 billion by 2050 [1-3]. Hitherto, saline water desalination has been the key to addressing the gap between the rising pure water requirements and the shortage of available resources [4]. Till now, desalination methods such as multistage flash desalination (MSF), multi-effect evaporator (MEE), and reverse osmosis (RO) are heavily employed globally. Nevertheless, these desalination systems are notorious for being extreme energy consumption. Furthermore, they pose an adverse impact on the environment due to the release of CO_2 gas [5]. For instance, the electrical energy consumption of RO approached 4–5 kWh/m^3 [6]. Conversely, the thermal energy consumption of MEE reached 30 kWh/m^3 [7] and that of MSF around 60–90 kWh/m^3 [8]. A comprehensive review of different existing water desalination systems that outlined their benefits and flaws was thoroughly discussed in [7,9,10]. As the energy price is soaring and the stringent roles on the use of fossil fuel are also intensifying, the search for less energy demanding desalination methods became inevitable. Authorities around the world are forcing industries and inventors to come up with novel ideas to reduce the energy utilization of desalination technologies. This situation induced research activity in the academic and industrial realms.

Accordingly, a palpable amount of research activities emanated in the literature addressing the enhancement of the energetic efficiency of the existing desalination technologies. For example, several reports have been engendered concerning the incorporation of renewable energy sources for water desalination purposes. Generally, solar and wind energies were the main sources utilized in water purification as they reduce energy costs and alleviate the greenhouse footprint. More details about the assessment and employment of renewable energy in the saline water purification industry can be found in review articles [11-13]. Similarly, to reduce the energy cost, several investigators proposed the implementation of low-grade energy sources. Low-grade heat sources are encouraging for freshwater production as they generate fewer greenhouse gasses and incur lesser costs [14,15]. Low-grade energy sources are available in many forms. For example, geothermal energy, spent industrial streams, and thermal

† To whom correspondence should be addressed.
E-mail: amkamal@ksu.edu.sa

fluid discharge [16,17]. Some discharged industrial fluids may have a temperature range of 50–90 ℃ [18]. Pappetrou et al. [17] have reported even a wider range where temperature can vary from 50 ℃ up to 1000 ℃ depending on the type of industry. Therefore, there is a high potential to run a desalination process by the rejected energy of alternative desalination/industrial systems. For instance, Chua et al. [6] proposed utilizing "waste" energy at a low temperature range of 65–90 ℃ to drive the multi-effect distillation (MED) process. They also introduced an alternate generation of the MED termed double-boosted MED (DBMED and flash-boosted MED (FBMED). The study proved the superiority of the modified versions over the conventional MED. In a continuous study, Chua et al. [19] conducted a thermos-economic evaluation of the amended MED structures. The study affirmed that the generated strains of MED provide lower water density costs relative to the typical MED. A Levelized water cost that varied from 0.9 to 1.3 $/m^3$ was reported. Similar studies that focus on the use of low-grade thermal energy for desalination purposes are reported in the open literature [5,16,20].

Alternatively, many investigators sought the reduction of energy consumption via joining different and/or similar desalination techniques to capitalize on the benefits and minimize the shortcomings of the individual system. This concept attracted innumerable efforts in the arena of academia and industry [21-23]. For example, Mitsos and Dahdah [24] generated a superstructure that coupled several blocks of MED-TVC, MED, and MSF subsystems. The size, structure, flow arrangement, and location of the vapor compression were optimized using sophisticated numerical methods. The objective function of the optimization was built on maximizing the gain output ratio and minimizing the scaled area of heat transfer. Helal [21] reviewed various integrated desalination methods and delineated their strengths and drawbacks. Hamed [22] studied and generated useful information about the present commercialized hybrid water purification systems. He shed light on and classified the hybrid systems based on the use of nano-filtration such as NF/MSF and NF/RO/MSF. Zak and Mistos [25] affirmed that the performance ratio (PR), recovery ratio (RR), and specific heat transfer area (*sA*) can be improved by coupling thermal desalination systems. Precisely, the study illustrated that hybridization of MSF with MEE processes boosted the performance ratio and recovery ratio values relative to the autonomous once through MSF (OT-MSF) unit. These successful results can be obtained even when the same operating conditions and number of stages and effects were employed. Almutaz et al. [26], and Ihm et al. [27] pointed out the existence of several large-scale commercial plants that integrated different desalination technologies. Indeed, these deployed plants integrated MSF and/or MEE with membrane technology such as reverse osmosis. Invariably, joining thermal desalination systems with membrane technologies rendered tangible benefits [21,22,25]. Tufa et al. [28] investigated the cogeneration of distillate water and electricity using a combined structure of membrane distillation and reverse electrodialysis desalination processes. The study revealed the possibility of achieving 83.6% water recovery at the expense of density power of 0.9–2.4 W/m^2. Farsi and Dincer [29] explored the energy and exergy efficiency of a poly-generation system that involved multi-effect distillation (MED) and direct-contact membrane distillation (DCMD). The proposed system was examined for the generation of pure water, electricity, cooling, and hydrogen. Similarly, Aly et al. [30] proposed a novel coupling of absorber composer with multi-effect desalination to reduced energy utilization and water price. The work revealed that a levelized water cost of 0.46 $/m^3$ and a performance ratio of 42% can be attained when the process operated at a top brine temperature of 65 ℃. Hesari et al. [5] proposed a hybrid process denoted as a cascaded multi-effect desalination system. They proved that by using less electrical energy the cascaded process can provide a 73% enhancement in the performance ratio compared to the standard MED. Lately, Capocelli and Barba [16] introduced a novel hybrid system to be driven by low-grade energy. The novel system was named FlashME which integrated MED with MSF in a compacted configuration. The novel system was compared with the conventional MED and with flash-boosted MED. The work revealed the superiority of the novel structure in the sense of increasing the distillate output by 20–28% over the flash-boosted MED and 100% over the traditional MED.

A modified version of the traditional MSF is known as Once-through MSF (OT-MSF). OT-MSF is a compact configuration that does not have the rejection section to reduce the capital and operational costs [31]. An extension of OT-MSF denoted as reversal MSF (MSFRV) was proposed and studied [32]. The MSFRV is theoretically analogous to OT-MSF, yet the flow direction is inverted. Reversing the feed flow permits the usage of naturally hot solution or saline water heated by low-cost energy sources. This feature entitles MSFRV to be run by low-grade energy resources. Ali et al. [32] affirmed that MSFRV can compete with OT-MSF in the sense of gain output ratio and normalized energy utilization. Yet, the study concluded that MSFRV exhibited a modest thermal efficiency and recovery ratio. As a remedy, Ali et al. [33] integrated MSFRV with membrane distillation. The results of the work revealed the opportunity to increase the recovery ratio from 7% to 23%, downgrade the scaled cooling water demand from 23 to 12 kg/kg, and shrink the energy utilization from 129 to 41 kWh/m^3 by the aid of hybridization. In the same line, Ali et al. [34] introduced the cascaded MSFRV to improve production and consequently reduce the specific energy demand. In their work, up to five blocks of MSFRV can be cascaded causing the recovery ratio to rise to 33.6% and the specific heat transfer area to descend to 327 $m^2/(kg/s)$ yet at the cost of inflated scaled energy demand of 320 kWh/m^3.

The previous studies of the MSFRV revealed its flexibility to be run by low-grade energy. It was also discovered that the reject brine recovered most of the input heat. Accordingly, the exergy of the MSFRV can be improved by harnessing the thermal energy accompanying the reject brine. This work aligns with the endeavors to develop an energy-efficient desalination technology via the integration of desalination methods and utilization of waste heat resources.

Specifically, the work aims to explore the integration of the MSFRV with MEE to exploit the thermal energy embedded in the reject brine. This means that the reject brine will act as the heat supplier to the MEE by emitting its sensible heat. Moreover, the entire hybrid system will be powered by a waste heat source. The waste heat could be industrial thermal waste, geothermal energy, exhaust steam, etc. Two hybrid structures will be analyzed. The two configurations differ in the way the internal energy is leveraged. The proposed systems will be assessed using well-known performance indicators such as recovery ratio, performance ratio, gain output ratio (GOR), specific energy consumption (SEC), and specific area of heat transfer. Furthermore, exergy analysis will be used to assess the efficiency of the proposed systems. The novel aspect of this work included integration of two low grade energy driven desalination system to enhance overall thermodynamic efficiency, utilization of boosters to increase distillate production to improve energy efficiency and conduction of exergy analysis to assess the efficiency of the proposed hybrid system.

2. Methodology

2-1. Reverse once through MSF (MSFRV)

Reverse MSF is a simplified version of the typical MSF as shown in Fig. 1a. The preheated seawater was fed to the bottom of the first stage, i.e., the flashing chamber. The seawater flashed into vapor and the remaining solution flowed to the next stage due to pressure difference. The brine kept flashing and losing its thermal energy as it passed through all stages. The brine departing the last stage was further quenched in the brine cooler by cooling water. The cold brine was then injected into the nth stage as a condenser stream. The condenser stream flowed through a condenser tube around which the flashing water condensed to formulate the distillate water. The condenser stream warmed up as it absorbed the heat of condensation. This procedure continued through all stages till the condenser stream exited the first stage at a high temperature. The condenser stream was discharged as a reject brine with an elevated temperature that reached a few degrees less than the feed temperature. Cooling the brine in the brine cooler was a crucial step because it created a temperature gradient between the flashing and condenser streams. It was essential to maintain such temperature differences throughout the stages because it worked as a driving force for flashing and condensation. One of the advantages of MSFRV was its suitability for being powered by low-grade/waste energy. Furthermore, the reject brine owned potential energy that can be leveraged to run another thermally driven desalination process.

The first principle model that described the underlying behavior of the MSFRV system has been fairly explained in the previous works [32, 35]. For this reason, the mathematical equations of the model were summarized as follows.

Mass balance around stage j

$$m_{b_j} = m_f - \sum_{i=1}^{j} m_{d_i} \tag{1}$$

Salt balance around stage j

$$m_{b_j} x_{b_j} = m_{b_{j-1}} x_{b_{j-1}} \tag{2}$$

Heat balance around stage j

$$m_{d_j} h_{fgj}(T_{v_j}) = m_{b_{j-1}} C_p (T_{b_{j-1}} - T_{b_j}) \tag{3}$$

$$T_{v_j} = T_{b_j} - BPR \tag{4}$$

$$A_{c_j} = \frac{m_{d_j} h_{fg}(T_{v_j})}{U_{cj} LMTD_{C_j}} \tag{5}$$

The distillate production rate:

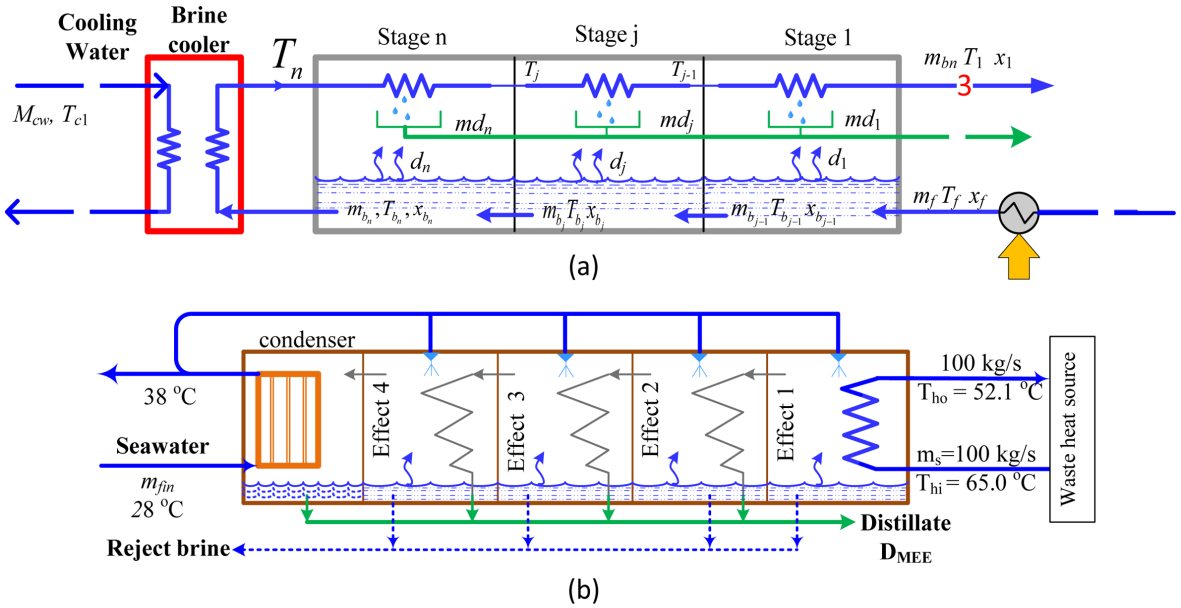

Fig. 1. Standalone MSFRV and MEE desalination systems.

$$D_{msf} = Total\ Distillate = \sum_{j=1}^{n} m_{d_j} \quad (6)$$

Heat balance around jth condenser tube [36]:

$$m_f(h_{c,j} - h_{c,j+1}) - \sum_{i=1}^{j} m_{d_i}(h_{d,j} - h_{d,j-1})_{x=0} - m_{d_j} h_{fg}(T_{v_j}) \quad (7)$$

Heat balance around Brine Cooler:

$$Q_{cool} = m_{cw} C_p (T_{c2} - T_{c1}) = m_b C_p (T_{bn} - T_n) \quad (8)$$

$$A_{bc} = \frac{m_{cw} C_p (T_{c2} - T_{c1})}{U_{bc} LMTD_{bc}} \quad (9)$$

$$LMTD_{bc} = \frac{(T_{bn} - T_{c2}) - (T_n - T_{c1})}{\ln\left(\frac{T_{bn} - T_{c2}}{T_n - T_{c1}}\right)} \quad (10)$$

$$T_{bn} = T_n + R_{cw}(T_{c2} - T_{c1}) \quad (11)$$

$$T_n = T_{c1} + DTC \quad (12)$$

$$T_{c2} = T_{c1} + dTc \quad (13)$$

Feed preheater:

The thermal energy required to power the process was estimated as follows:

$$Q_{heat} = m_f C_p (T_f - T_{fo}) \quad (14)$$

As mentioned earlier, seawater can be heated by waste/free heat source. Thereby, Eq. (14) would be utilized only to measure the heating load demand. In the above equations, A_c denoted the heat transfer area of the condenser tube. The total required heat transfer area of MSFRV would be the accumulation of the area of all tubes.

To simulate the above mathematical equations of the MSFRV, specific design parameters must be predefined. Here, the definite parameters were the number of stages (n), feed salinity and temperature (x_f, T_f), the seawater feed flow rate (m_f), the coolant mass ratio (R_{cw}), the coolant inlet temperature (T_{c1}), the cross-temperature drop (DTC), and the temperature drop at the coolant side (dTc). Recall that dTc signified the temperature gradient at the coolant side. Hence it determined the cooling demand for an assigned R_{cw}. Similarly, DTC specified the magnitude of T_n. Accordingly, R_{cw} adapts T_{bn}. By fixing T_{c1}, DTC, and dTC, the terminal temperatures, i.e., T_n, and T_{bn} can be computed using Eq. (11-12). By computing T_n and T_{bn}, estimation of the stage-to-stage temperature of the flashing chamber and condenser tube can be facilitated. Insofar, the unspecified parameters were the brine temperature for the n stages, the condenser temperature for the n stages, and the feed flow rate, m_f. The organigram for solving the modeling equations was explained in previous works [32,35]. In addition to the prespecified variables, two additional terminal temperatures defined. They were the feed temperature (T_f) and the condenser temperature entering the last stage (T_n). Since T_n was linked to T_{c1} and the heat exchanger efficiency manifested by R_{cw}, T_{bn}, and T_1 were left as free variables. Supplementary equations that defined the physical properties of the water solution were given in Appendix A.

2-2. Multi effect evaporators (MEE)

The standard MEE process is presented in Figure 1b. The displayed MEE process used sensible heat instead of steam to power the evaporation [5,6]. This was essential here because the MEE would be powered by the sensible heat of the MSFRV spent brine. The process has a parallel feed structure where the seawater was apportioned into equal streams and sprayed into the top of each effect. Before spraying, the seawater intake was preheated in the down condenser to condense the vapor of the last effect. In the first effect, a fraction of the seawater feed evaporated due to the released sensible heat. The remaining brine is rejected at the bottom of the effect. The produced steam passed to the next effect where it acted as an energy source. This steam condensed due to the injection of fresh seawater feed and constituted the distillate product. The released latent heat created another vapor from the fresh feed. This process was repeated in each effect. In the last effect, the generated vapor was then condensed in the down condenser to produce distillate and preheat the seawater intake.

The mathematical equations describing MEE physics are excellently reported in the literature [37-40]. Similarly, the details of the MEE mathematical expressions were presented in a previous work [41]. Therefore, the modeling equations were summarized here considering minor adjustments of the first effect to include the use of sensible heat to run the process [4, 6, 20]. The conservation law for mass, salt, and energy and the heat transport mechanism in the first effect was expressed as follows:

$$F_1 = B_1 + V_1 \quad (15)$$

$$X_f F_1 = X_1 B_1 \quad (16)$$

$$m_s Cp(T_{h_i} - T_{h_o}) = V_1 \lambda_1 + F_1 Cp(T_{b_1} - T_f) \quad (17)$$

$$m_s Cp(T_{h_i} - T_{h_o}) = U_1 A_1 (T_{ho} - T_{b_1}) \quad (18)$$

In the above equations, F_1, B_1 and V_1 designated the feed, brine, and vapor flow rate of the first effect, respectively and X_1 was the salinity in the first effect. X_f, T_f stood for the salt concentration and temperature of the feed. m_s, T_{hi}, T_{ho}, and λ_{v1} denoted the flow rate of the heating source, the inlet temperature of the hot source, the outlet temperature of the hot source, and the latent heat of the steam at T_{v1} (vapor saturation temperature in the first effect), respectively. T_{b_1}, U_1, and A_1 signified brine temperature, heat transfer coefficient, and heat transfer area of the first effect. The term $T_{hi} - T_{ho}$ represented the temperature change in the sensible heat of the MEE heat supplier. This term was a crucial design parameter and denoted as ΔT_{sen}.

For any effect i between 2 and n, Eqs. (15-18) were rewritten as follows:

$$F_i = B_i + V_i \quad (19)$$

$$X_f F_i = X_i B_i \quad (20)$$

$$V_{i-1}\lambda_{i-1} = V_i \lambda_i + F_i Cp(T_{b_i} - T_f) \quad (21)$$

$$V_{i-1}\lambda_{i-1} = U_i A_i (T_{v_{i-1}} - T_{b_i}) \quad (22)$$

The generated distillate water was described as follows:

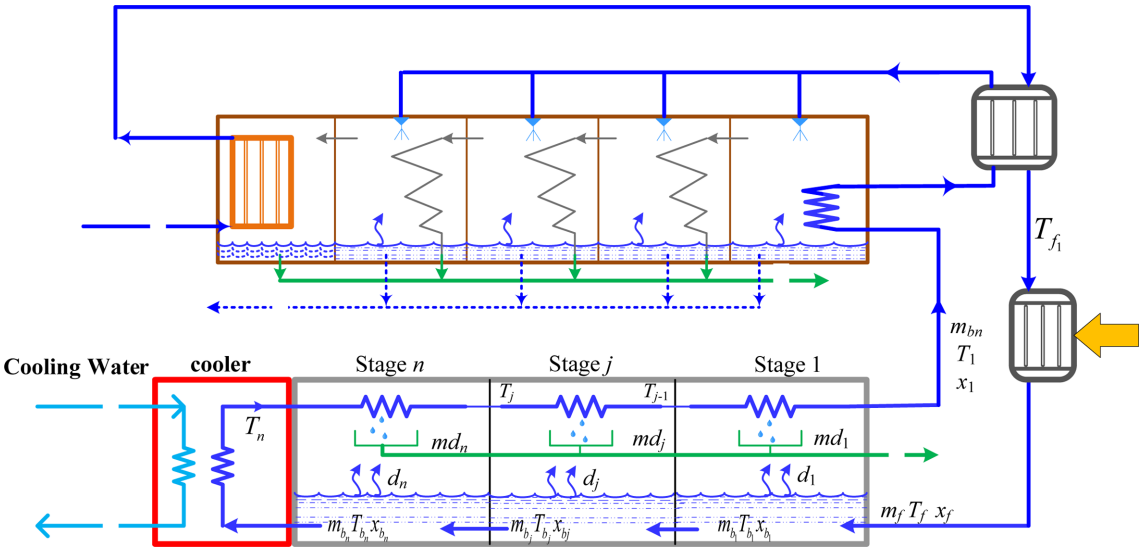

Fig. 2. MSFRV-MEE hybrid structure (HYB).

$$D_i = V_i;\ i = 1, \ldots, n \tag{23}$$

F_i, B_i, V_i, and D_i signified the feed, brine, vapor, and distillate flow rate of the ith effect, respectively. X_i was the salinity in ppm of the ith effect. T_{b_i} snd T_{v_i} denoted the brine and vapor temperatures of the ith effect, respectively. λ_i, U_i and A_i stood for the latent heat, heat transfer coefficient, and heat transfer surface area of the ith effect. The gross area of heat transfer for MEE was hence the accumulation of all effect's area. The brine, vapor, and condensate temperatures in each effect were linked as follows:

$$T_{v_i} = T_{b_i} - BPR_i \tag{24}$$

$$T_{d_i} = T_{v_i} - \Delta T_c \tag{25}$$

In Eq. (25), T_d represented the distillate temperature and ΔT_c was a correction factor that took care of pressure and friction losses.

The heat balance around the down condenser can be written as follows:

$$D_n \lambda_n(T_{v_n}) = m_{f_{in}} Cp(T_f - T_{cw}) = U_{dc} A_{dc} LMDT_c \tag{26}$$

Where:

$$LMDT_c = \frac{T_f - T_{cw}}{\ln\left(\frac{T_{d_n} - T_{cw}}{T_{d_n} - T_f}\right)} \tag{27}$$

The required heat transfer area for the down condenser can then be calculated using Eqs. (26) and (27).

2-3. Description of the hybrid systems

The standalone MSF and MEE systems were presented in the previous sections. The coupling of these methods to create a hybrid system was explained here. Moreover, the hybrid system would be powered by a low-grade/waste energy source. The main incentive of hybridization was to harvest of the thermal energy inherited with the reject brine of the MSFRV system. Hence the overall energy efficiency of the proposed hybrid system can be improved. Different possible hybrid structures can be generated. In this work, two configurations were proposed as shown by Figs. 2, 3 denoted as HYB and BHYB structures. For both structures, the brine solution was injected into the MSFRV. The spent brine exiting the MSFRV was directed to the MEE to serve as the sensible heat supply and feed stream. For both configurations, external waste energy is employed to power the overall system. The waste energy was utilized to heat the primary feed of the system. In the HYB system, the seawater to be treated, named as the primary feed, was preheated in a heat exchanger (HE01). This action minimized the intake of energy from the waste energy source which further improved the energy efficiency of the hybrid system. Usually, waste energy is deemed free, but it is meaningful to evaluate the energy requirement for comparison and analysis. Moreover, the HYB system contained a brine cooler that used external cooling water.

To achieve a more efficient structure with the least cooling and heating requirements, the boosted hybrid system (BHYB) was proposed (Fig. 3). The BHYB structure had a remarkable modification where the brine cooler and HE01 were replaced by booster units, namely B1 and B2. The boosters have a dual function. One function was to serve as a cooler, i.e., cooling the MSFRV warm brine using B1, and cooling the warm brine before entering the MEE using B2. The second function was to produce additional vapor that can be used as a booster for the MEE system. The booster was a simple evaporator unit where a sub-atmospheric brine solution can be vaporized by a sensible heat operating at a relatively higher temperature than the brine solution itself. The vapor can be condensed as distillate water. However, its energy was judicially leveraged as an energy source to be injected into a proper location in the MEE process. Hence, this added vapor would boost the evaporation of the designated location (effect). The steam generated from B1 would be of a low-temperature

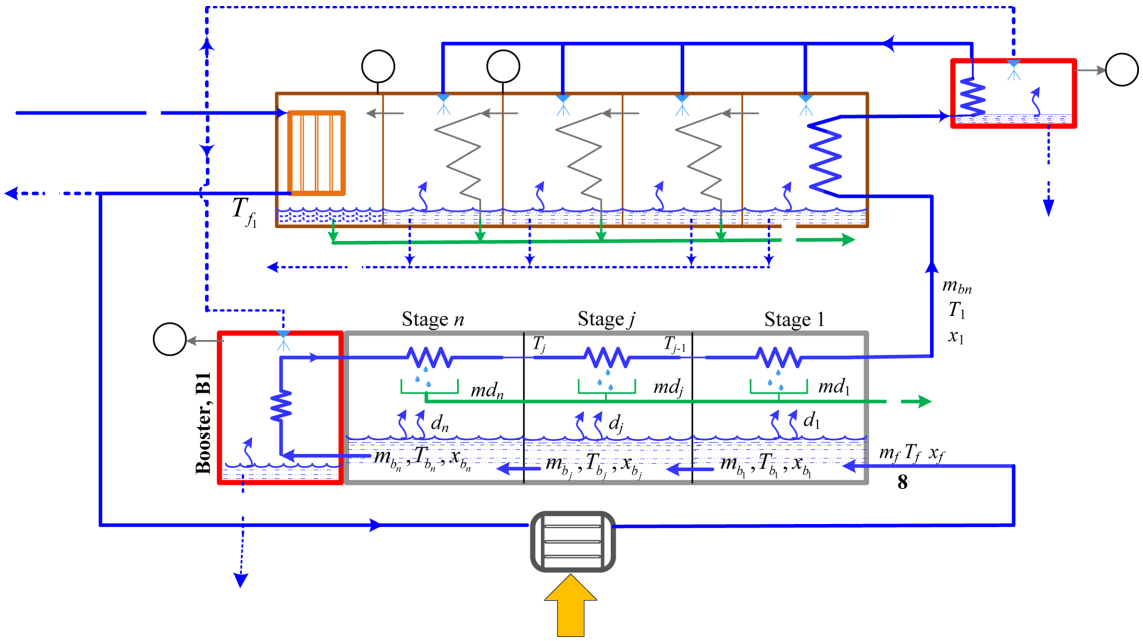

Fig. 3. MSFRVT_F1 -MEE hybrid structure with booster (BHYB).

grade that cannot be used as a booster. Thus, it was injected into the down condenser for condensation. The generated steam in B2 would be injected at the appropriate effect location as a booster. Note the boosters needed a liquid brine to generate the steam which was taken from the main seawater intake. In due course, B1 leveraged the energy of the MSFRV brine to produce additional distillate. Similarly, B2 harnessed the energy of the brine exiting the MEE heat supplier to produce additional distillate and at the same time boost the original MEE system. The flow rate of the primary feed (m_f) would be kept equal for both structures for just comparison. However, for the BHYB system, a portion of the seawater would be directed to B1 and B2, which was estimated based on the proposition of feed to vapor ratio of 2.2 [5]. This structure was expected to eliminate the auxiliary cooling requirement and increase water production via the boosters.

Table 1. Operating conditions

Parameter	Value
m_f	5920 kg/s
x_f	35000 ppm
T_{fo}	25 C
T_f	80 C
T_{c1}	25 C
dTc	10 C
$dTcw$	8 C
DTC	5 C
DTh	15 C
n	24
ne	4
H_{ef}	0.8
x_b	70000 ppm
R_{cw}	1.1
ΔT_c	0.5 C

2-4. Numerical simulation of the hybrid systems

Organigram that described the simulation of the hybrid structures was demonstrated by Figs. B.1 and B.2 in Appendix B. Specific design parameters must be defined such as the seawater flow rate, temperature, and salinity (m_f, T_{fo}, x_f), the MSFRV feed temperature, T_f, the MSFRV number of stages n, the MEE number of effects, ne, HE01 effectiveness Hef, the coolant inlet temperature, T_{c1}, the coolant to brine ratio, R_{cw} the temperature drop at the coolant side, dTc, the temperature drop at the brine side DTC, and the temperature drop at the MEE heat supply, $\Delta T_{sen} \equiv DTh = T_{hi} - T_{ho}$. For the BHYB, an additional design parameter, $dTcw$ which denoted the temperature drop at the seawater side of C1 was introduced. The default magnitude of these parameters was listed in Table 1. In this work, the lower bound of Tho was 45 ℃ to ensure elevated top brine temperature (TBT) that furnished acceptable overall temperature drop across the MEE unit to expand the evaporation over the whole effects. Additionally, the temperature for the last effect was bounded by 400 ℃ to guarantee a meaningful temperature difference between the vapor and the condenser stream (seawater). This temperature was also constrained by the sink temperature, i.e., the temperature of the cooling water used in the down condenser. Additionally, the top brine temperature in the MEE must be less than the outlet temperature (T_{ho}) of the MEE heater by the temperature of the approach. A temperature of approach of 20 ℃ was adopted in this study [42]. Moreover, the MEE feed temperature (T_{ff}) must be maintained marginally lower than the temperature of the last effect. It should be noted that the temperature of the MSFRV feed (T_f) was denoted as the primary feed temperature.

The hybrid system (HYB) included an additional heat exchange (HE01). The necessary heat transfer area of HE01 can be calculated

as follows:

$$A_{bh} = \frac{m_{b_n} Cp(T_{hi} - T_{ho})}{LMTD_{bh}} \tag{29}$$

$$LMDT_{bh} = \frac{(T_{ho} - T_{f1}) - (T_{hc} - T_{fo})}{\ln\left(\frac{T_{ho} - T_{f1}}{T_{hc} - T_{fo}}\right)} \tag{30}$$

Since the booster was conceptually a secondary effect, the size of the boosters can be estimated the same way the area of the MEE effect was calculated. Several key performance indicators (KPIs) would be used to assess the performance of the proposed systems. The KPIs were listed in Appendix A. Simulation of the proposed models was carried out using MATLAB.

2-5. Exergy principles

Exergy is a thermodynamic index that assesses the theoretically extractable work of a given system when it rests at a steady state. Exergy balance can provide insightful information about the effectiveness of a process at equilibrium. This knowledge can define specific parts of the process that may require enhancements or modification. Furthermore, it can be used as a performance indicator for efficiency improvements towards sustainable development [41,42]. So far, Exergy was a helpful tool to gauge and/or compare the energy efficiency of different processes or different configurations of a single process. Exergy can be computed as [41, 42]:

$$E = (H - H_0) - T_o(S - S_0) + \sum_{i=1}^{i=k} w_i(\mu_i - \mu_{i,o}) \tag{31}$$

H_0 and S_0 represented the enthalpy and entropy values at the reference temperature and pressure T_0, P_o which were taken to be 298 K and 1 atm, respectively. H and S stood as the enthalpy and entropy at a specified temperature, T (K). w was the mass fraction and m was the chemical potential at the reference temperature and pressure. The subscript "o" denoted the chemical potential calculated at the reference concentration xo, which was taken as 0 ppm in this study. k was the number of chemical components within a stream. The chemical potential of salt in water was estimated using the MATLAB code developed by the research group at MIT [43,44]. Since all inlet and outlet streams were operating at low atmospheric pressure, the impact of pressure on exergy was neglected.

Verily, all processes converted energy into work and consume exergy. Usually, energy was always balanced, while, for realistic systems, exergy was never balanced due to irreversibility, i.e., entropy generation or exergy destruction. The exergy destruction, ΔE, showed existing work that can be properly leveraged for potential process upgrades. In Engineering applications, the exergy destruction or loss can be expressed in a unified form as follows:

$$\Delta E = \sum_{i=1}^{n} m_i E_i - \sum_{o=1}^{k} m_o E_o + Q\left(1 - \frac{T_o}{T}\right) - W \tag{32}$$

m_i and m_o represent the inlet and outlet mass flow of the system, Q is input heat to the system, E_i and E_o denoted the specific Exergy for input and output streams respectively, and W work done on the system. n was the number of input streams and k was the number of output streams.

For the adiabatic system ($Q = 0$) and since no work was involved ($W = 0$), then Eq. (32) became:

$$\Delta E = \sum_{i=1}^{n} m_i E_i - \sum_{o=1}^{k} m_o E_o \tag{33}$$

Martinaitis et al. [43] studied how the choice of reference temperature can genuinely influence the exergy analysis. In this study, the reference state was considered as $T_0 = 298$ K; $P_0 = 1$ *atm* and salinity = 0. Such conditions simulate the environment. Another way to compare the system's effectiveness was through exergy efficiency. Typically, the exergy efficiency is defined as [43]:

$$\eta_{ex} = \frac{\Delta E}{E_{inp}} \tag{34}$$

Estimation of exergy destruction and exergy efficiency can help in analyzing the process performance and efficiency. Particularly. These metrics would be used to compare the effectiveness of the proposed configurations. Therefore, the configuration with the best utilization of energy can be identified. Significant energy savings by reducing exergy losses via design modification can be assessed.

3. Results and Discussion

Verification of the MSFRV model has been discussed in earlier work [32]. To save space, validation was excluded here. Likewise, the MEE model was authenticated previously [41]. However, the previous validation was based on the steam-driven MEE system. To assess the current model with that powered by sensible heat, the case study in [6,45] was selected for verification. The operating condition for the selected example was given in Fig. 1b. The result of the comparison was delineated in Table 2. Indeed, the performance ratio (PR) and production rate of the present model were compared against that of Rahimi et al. [45]. Note that the performance ratio for waste heat was defined by Rahimi et al. [45] and defined by Eq. (A.10) in Appendix A. The average discrepancy in the estimated PR was 10%

Table 2. Validation of the MEE model using sensible heat source

T_{hi} (C)	65	70	75	80	85	90
ne	4	4	5	5	6	6
PR [45]	1.18	1.473	1.773	2.029	2.301	2.529
PR [this work]	1.26	1.6	1.95	2.23	2.58	2.98
Production (m^3/day) [45]	707	998	1341	1694	2103	2573
Production (m^3/day) [this work]	689	996	1358	1718	2181	2731

while that for the production rate was 2%. The mismatch in the prediction can be attributed to the difference in predicting the supporting physical properties. Yet, the prediction precision was sufficient to analyze the hybrid systems. Afterward, the effectiveness of the proposed hybrid structures would be examined. Verily, the number of effects and temperature drop per effect were interrelated and bounded to the top brine temperature since the temperature of the last effect is fixed. Both have a profound impact on the performance. Indeed, *dT* had a complex effect on the evaporator behavior and its impact may change with the degree of the deviation between the feed and the effect's temperatures. Hence the following analysis will be based on fixing the differential temperature *dT* while the number of effects was allowed to vary with TBT. In fact, expanding *ne* had a steady and predictable effect on evaporation. Furthermore, it led to enhanced leverage of the existing energy.

3-1. Comparison of the proposed hybrid systems

A comparison of the proposed hybrid systems with the standard MSFRV was shown in Fig. 4. The results were based on fixed operating conditions; primary feed temperature of 80 ℃, temperature drop per effect of 1 ℃, temperature drop of 15 ℃ for the sensible heat, and 24 stages for the MSFRV. Undoubtedly, both the HYB and BHYB systems outperformed the standalone MSFRV over almost all aspects by many folds. Exceptionally, the standard MSFRV had the lowest specific area despite its very low production rate because the hybrid structures contained additional evaporators, a down condenser, and a heat exchanger. Note that for $dT = 1$ ℃, a total of 19 effects were incorporated into the MEE system. Nevertheless, the basic system recovery ratio was 6.8, HYB's was 31.3, and BHYB's was 45, so this was equivalent to 360, and 561% improvement, respectively. The baseline SEC was 1076 kW/m^3, HYB's was 145 kW/m^3, and BHYB's was 94 kW/m^3 which was equivalent to 85–91% reduction, respectively. The baseline GOR was 0.8, HYB's was 6.6, and BHYB's was 7.7 which was equivalent to 725–837% enhancement, respectively. The baseline PR was 0.7, HYB's was 3.3, and BHYB's was 5.3 which is equivalent to 371–675% improvement, respectively. The basic case-specific cooling water consumption was 15.7, HYB's was 3.4, and BHB's was 0.0 which was equivalent to a 78–100% reduction, respectively. Of course, the enhanced KPIs were related to the augmented production of distillate water without additional energy supply. In addition, the BHYB was found to be superior to the HYB system as a 59% greater production rate was obtained. The escalated production rate was ascribed to the aid of the boosters to produce more vapor. The augmented production rate of the BHYB system improved its corresponding KPIs relative to the HYB system. For example, the BHYB system has 12% and 35% less *sA* and SEC, respectively. Moreover, it owned 12% and 60% higher GOR and PR, respectively. Additionally, the BHYB structure did not require auxiliary cooling water.

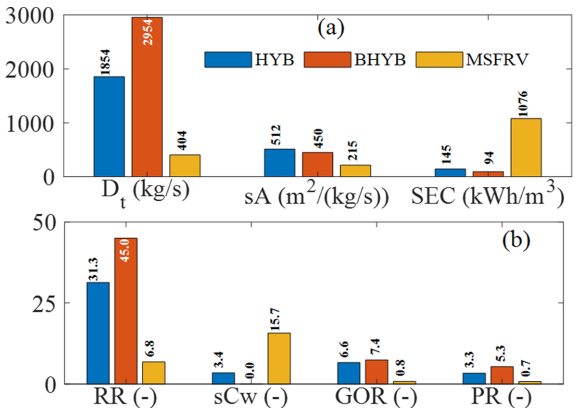

Fig. 4. Comparison of the performance of the proposed hybrid systems; T_f = 80 ℃, n = 24, dT = 1 ℃, ΔT_{sen} = 15 ℃.

3-2 Effect of primary feed temperature

The temperature of the saline feed to the hybrid system, T_f was a vital design parameter because it affected the performance of both the MSFRV and MEE. T_f influenced the MSFRV directly and MEE via T_{hi} which was equal to T_1, the temperature of brine exiting the MSFRV. Fig. 5 compared the two hybrid structures at a range of primary feed temperature but at constant differential temperature of 1 ℃ and ΔT_{sen} = 15 ℃. It should be recalled that at a feed temperature less than 70 ℃, a value of 15 ℃ for ΔT_{sen} was not possible because it incurred T_{hi} to be less than 45 ℃. In this case, ΔT_{sen} was adjusted such that T_{hi} stayed equal or higher than 45 ℃. By fixing dT and ΔT_{sen}, the utilized number of effects increased with T_f. This generated better use of the supplied energy to produce additional vapor in the MEE system. Furthermore, increasing the primary feed temperature enhanced the distillate production of the MSFRV system as the input energy intensifies. The combined elevated production of the MEE and MSFRV generated a proportionally growing overall recovery ratio (Fig. 5a) for both HYB and BHYB structures. Surely, a 54% recovery ratio can be attained at the highest feed temperature for the BHYB structure. Fig. 5b illustrated the evolution of the normalized

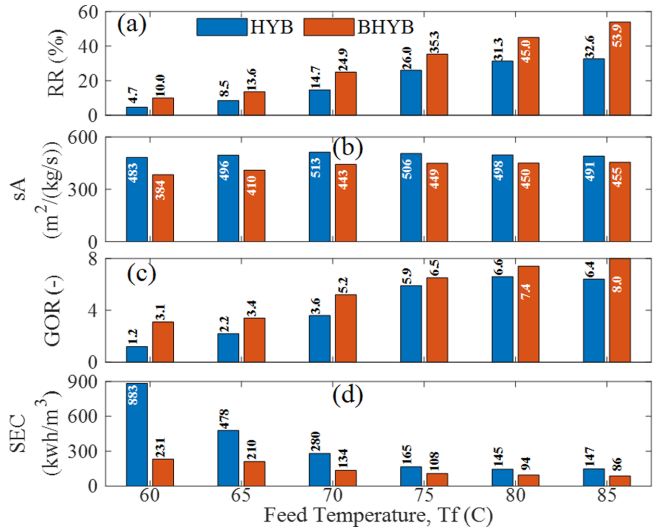

Fig. 5. Effect of T_f on the performance of the hybrid systems; ΔT_{sen} = 15 ℃, n = 24, dT = 1 ℃

surface area with feed temperature. Essentially, the required heat transfer area increased with feed temperature because both the MEE vapor production and the number of effects grew with T_f. For BHYB, *sA* raised with feed temperature, however, the growth rate is dampened because of the rapidly growing production rate. For the HYB system, the specific area had a concave trend, i.e., it increased up to T_f = 70 ℃ and then declined afterward. This is because the required surface area and production rate evolved at different rates. Fig. 5c depicted the GOR profile with respect to variations in the feed temperature. For BHYB, GOR improved proportionally with feed temperature because of the linearly escalating vapor production. Note that the heat supplied by the waste energy increased with feed temperature. Despite the growing heat supply, GOR kept rising. This was because the growth in vapor production surpassed the growth in the heat input. For HYB, GOR also evolved with feed temperature, but it dipped at 85 ℃. As mentioned earlier, the heat supply increased with feed temperature while the vapor production of the HYB system grew monotonically as manifested by the trend of *RR* shown in Fig. 5a. As a result, the generated profile of GO Rimproved slowly and declined at the end. Figure 5d demonstrated the variation of the specific energy consumption with primary feed temperature. The energy consumption of the hybrid system aroused from the heat supplied by the waste heat source. For the HYB system, additional energy consumption was inquired by the MSFRV brine cooler. Generally, the energy consumption evolved with feed temperature because the heat supply was proportional to the difference between the primary feed temperature and T_{f1}. Therefore, the energy consumption raised linearly with primary feed temperature. However, due to the progressive evolution of the production rate, the specific energy consumption reduced substantially with primary feed temperature. The reduction in SEC was gradual for the BHYB system but swift for the HYB system. Recalling that the energy consumption of the HYB system was higher than that of BHYB because the former included the cooling duty. Interestingly, the specific energy consumption was dramatic for the HYB system at low feed temperatures. Interestingly, the specific energy consumption was dramatic for the HYB system at low feed temperatures due to the higher cooling duty at lower feed temperature the cooling duty at lower feed temperatures. Recall that at low feed temperatures, the MSFRV production was minimal and subsequently, the flow rate of the brine circulating inside the brine cooler was greater incurring further cooling duty. This grown energy consumption was further inflated by the relatively reduced total production rate at feed temperature of 60 and 65 ℃. Nevertheless, Fig. 5 illustrated the superiority of the BHYB structure relative to the HYB structure with respect to all KPI's.

3-3. Effect of sensible heat temperature drop

The temperature gradient of the MEE sensible heat, ΔT_{sen} was a significant design parameter. This parameter particularly affected the MEE performance. Nonetheless, it significantly influenced the overall performance because the MEE production had a significant share of

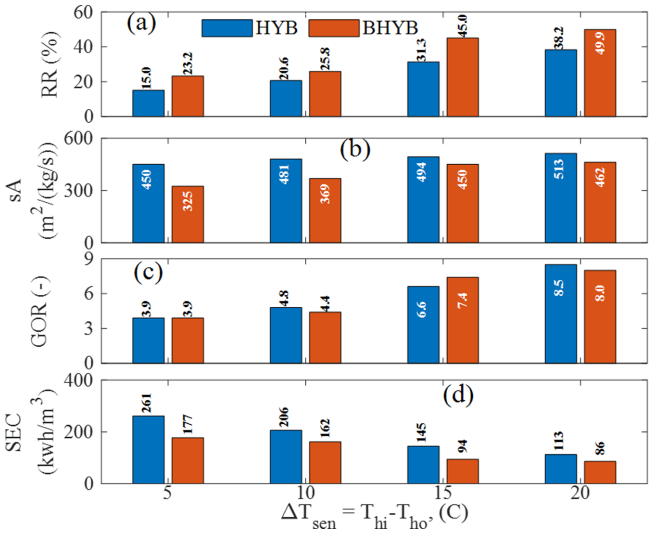

Fig. 6. Effect of ΔT_{sen} on the performance of the hybrid systems; T_f = 80 ℃, n = 24, dT = 1.

the total production. Verily, ΔT_{sen} regulated the quantity of the heat released from the MEE heater and accordingly the volume of distillate production. Elevated ΔT_{sen} generated greater sensible heat supply, but lesser top brine temperature. Smaller TBT reduced the total number of effects that can be used when dT was fixed, which was the case here.

Fig. 6 displayed the impact of ΔT_{sen} on the performance of the hybrid structures when the differential effect temperature was fixed at 1 ℃ and the primary feed temperature was set at 80 ℃. The positive effect of increasing ΔT_{sen} on the production rate was obvious in Figure 6a for both the HYB and BHYB systems. Elevating the temperature drop improved the vapor production although the top brine temperature and consequently the number of effects decreased. This affirmed that ΔT_{sen} had a more profound impact on MEE production than TBT. Fig. 6b depicted the reaction of the specific heat transfer area to the evolution of the temperature drop. Clearly, *sA* raised slowly with ΔT_{sen} for both hybrid structures. The total required heat transfer area grew with ΔT_{sen} mainly due to the escalating vapor production. However, since the production rate increased with ΔT_{sen}, the trend of the normalized surface area became asymptotic. The enhancement in production rate with ΔT_{sen} was reflected in the GOR trend as illustrated in Fig. 6c. For both hybrid systems, GOR enhanced but at different rates. The different rate of growth of GOR was related to the different rates of growth in production rate and heat supply. For BHYB, the waste heat supply rate was constant because both T_f and T_{f1} were invariant. For the HYB system, the waste heat supply was relatively smaller but continuously raised with ΔT_{sen} because T_{ho} reduced as well as T_{f1}. Finally, the progress of specific energy consumption with regard to rising ΔT_{sen} was typified in Fig. 6d. Obviously, SEC diminished as the temperature drop elevated primarily because of the enhanced production rate. Note that for the BHYB system, the energy consumption was constant because the supplied waste energy was constant as both T_f and T_{f1}

were invariant with ΔT_{sen}. Alternatively, for the HYB system, the waste heat supply increased because T_{f1} decreased with ΔT_{sen}. The heat supply was further augmented by the cooling duty making the total energy consumption of the HYB system larger than that of the BHYB system. Consequently, the corresponding specific energy consumption of the HYB system became higher than that of the BHYB system. Once again, Fig. 6 proved the supremacy of the BHYB structure over the HYB structure with regard to all KPI's.

3-4. Effect of the temperature drop per effect

The previous analysis was based on a differential temperature per effect of 1 ℃. According to Rahimi et al. [42] the design effect-to-effect temperature drop was between 2 and 4 ℃. Under cost consideration, the temperature drop across each effect can be between 1.5 to 2.5 ℃[20]. For this consideration, Fig. 7 depicted the variation of the KPIs when dT varied between 1 and 4 ℃. In this case, the primary feed temperature was fixed at 80 ℃ and the temperature drop of the sensible heat was set at 15 ℃. As expected, as dT increased, the associated number of effects decreased compromising the full utilization of the available heat energy. As a result, the production rate declined and so did the recovery ratio. This adverse impact was also manifested in energy-related KPIs such as GOR and SEC (Fig. 7c, d). Considering both hybrid structures, both GOR and SEC worsen as the differential temperature increased. Since the feed temperature and the temperature drop of the sensible heat were fixed, the GOR decreased following the declining production rate. The same argument applied to the SEC. The only benefit of increasing dT was the reduction of the normalized surface area as shown in Fig. 7b. Normally, expanding dT, which was associated with shrinking the number of effects, would definitely acquire less total heat transfer area. As the decline in the total area was sharper than the incline of the production rate, the resulting normalized area descended.

3-5. Operability range

Clearly, both the primary feed temperature and the temperature drop of the sensible heat affected TBT and subsequently the number of effects but oppositely. To investigate the operation range of the hybrid system, we simulated the system at different values for T_f and ΔT_{sen} exclusively for the BHYB system. Fig. 8 showed the outcome of this investigation using dT = 1 ℃. Specifically, Figure 8a illustrated how the number of effects changed with these parameters. Verily, ne raised with T_f and declined with ΔT_{sen}. Noting that the smallest temperature drop of 5 ℃ can be applied to the entire temperature range of the primary feed. Conversely, the largest temperature drop of 20 ℃, can be implemented only for feed temperature equal to or higher than 75 ℃ due to the temperature gradient across the MSFRV and the minimum allowable value for T_{ho}. These ranges of ne were dictated by the obtained top brine temperature shown in Figure 8b. Remarkably, TBT equaled the feed temperature minus the sum of the temperature drop across the MSFRV, the temperature drop on the sensible heat and temperature of approach. Consequently, the smallest ΔT_{sen} generated the largest TBT and vice versa. For this reason, the smallest ΔT_{sen} owned the greater operation range. The operation range decreased with ΔT_{sen} because of the lower bound on T_{ho}. The distribution of TBT and ne over the operation range created variable performance as demonstrated in Fig. 8c, d. Specifically, Figure 8c delineated the response of the recovery ratio. For the smallest temperature drop, the recovery ratio raised with feed temperature because of the inclining number of effects but at a low rate because it possessed the lowest heat input. As ΔT_{sen} grew the supplied sensible heat ascended as well as the resulting recovery ratio. Of course, the trend of ΔT_{sen} = 20 ℃ should have the largest and fastest-growing recovery ratio. Despite its higher input heat, it can have the same recovery ratio of ΔT_{sen} = 15 ℃ at T_f = 75 ℃ because its number of effects was smaller than that of ΔT_{sen} = 15 ℃. This means at dT =

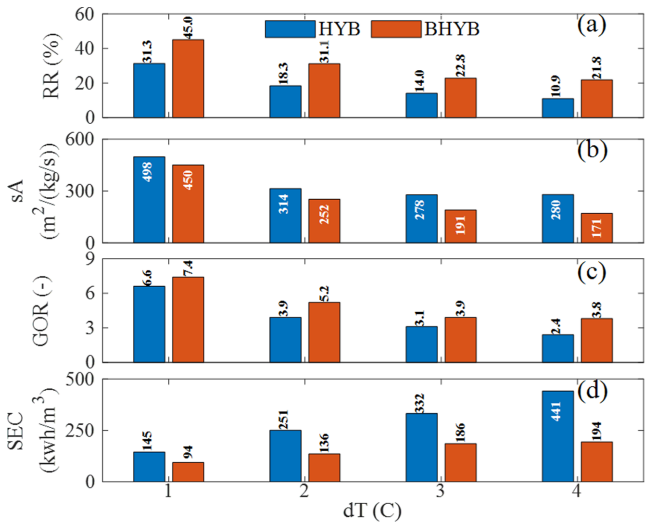

Fig. 7. Effect of dT, the temperature drop per effect, on the performance of the hybrid systems; T_f = 80 ℃, ΔT_{sen} = 15 ℃, n = 24.

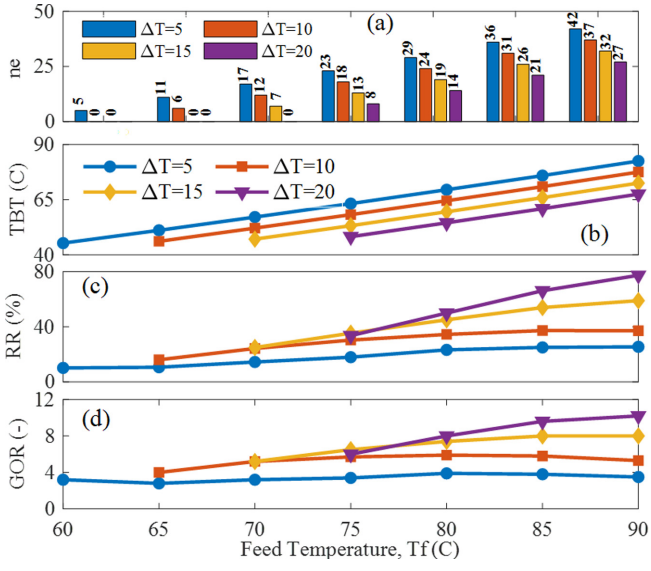

Fig. 8. Combined effect of T_f and ΔT_{sen} on the performance of BHYB structure, n = 24, dT = 1 ℃.

1 ℃ and $ne = 8$, the input energy at $\Delta T_{sen} = 20$ ℃ was inefficiently leveraged. Fig. 8d showed the response of GOR which basically followed the *RR* profile. The input energy from the waste source indeed increased with feed temperature, but it was unified for all cases. Hence, the increment in GOR was purely due to the evolution of the supplied sensible heat with ΔT_{sen}. However, the growing waste energy intake either showed down the growth of GOR as in ΔT_{sen} = 15 & 20 ℃ or declined the GOR as in ΔT_{sen} = 5 & 10 ℃.

3-6. Effect of temperature drop at the MSFRV brine cooler

The temperature drop at the brine cooler (*dTc*) of the MSFRV played an important role in the performance of the MSFRV and consequently on the MEE via the reject brine temperature. The latter worked as the inlet temperature to the MEE sensible heat supplier. In the previous analysis, *dTc* was fixed at 10 ℃. It was interesting to study its impact on the process. Specifically, its reflection on the BHYB structure would be examined. Although BHYB had a booster instead of a cooler, the concept still applied. Fig. 9 displays the reflection of the *dTc* variation on the performance of the BHYB system. As shown by Figure 9a, as *dTc* raised at fixed T_n, the brine temperature at the last stage (T_{bn}) increased accordingly. In fact, T_{bn} surged from 38 to 54 ℃ causing a smaller overall temperature drop in the MSFRV unit. Hence, improper harness for the energy supplied to the MSFRV occurred at high values of *dTc* degrading the production of the MSFRV (Fig. 9b). Another consequence was that the reject brine temperature of the MSFRV declined sharply causing the inlet temperature of the MEE heater (T_{hi}) to descend proportionally. This, in turn, reduced TBT proportionally with a fixed difference. Note that the difference between TBT and T_{hi} was the sum of the temperature of approach and ΔT_{sen}. The latter was fixed at 15 ℃ in this simulation. The fast drop in TBT generated a sharp decline in the MEE production as shown in Fig. 9b. At the lowest *dTc* of 8 ℃, T_{hi} closely approached the primary feed temperature (T_f) leading to exponential growth in the heat transfer area of the MSFRV unit. Reducing *dTc* further was impossible because it necessitated a huge

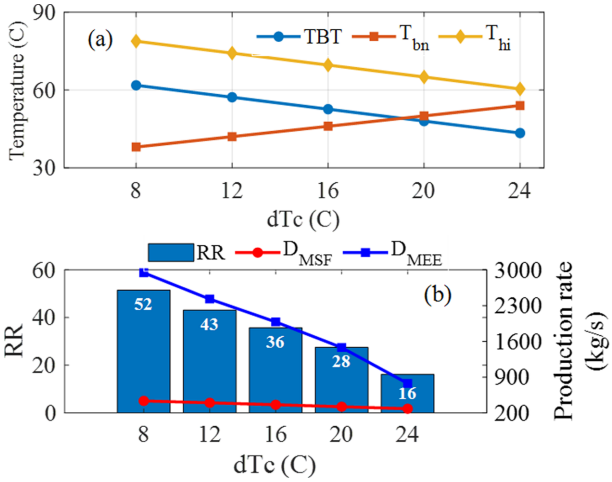

Fig. 9. Effect of the brine cooler capacity on the performance of BHYB structure, T_f = 80 ℃, ΔT_{sen} = 15 ℃, n = 24, dT = 1 ℃.

amount of heat to be transferred to the MSFRV condenser tube which was thermodynamically not possible. On the other side, at the largest value of *dTc* of 24 ℃, TBT became equal to 45 ℃ which was the lowest permissible value. Beyond this value the operation of the MEE became useless. The situation was even worse for smaller primary feed temperatures as the safe range for *dTc* became narrower. Fig. 9b showed the effect of the TBT and T_{bn} variation, which was induced by the variation of *dTc*, on the production rate and consequently the recovery ratio. The production of the MSFRV declined but was not clearly visible because of its smaller scale compared to the MEE production. Similarly, the MEE production decreased rapidly because of the declining TBT. Note that smaller TBT created a lesser overall temperature drop across the MEE unit and consequently marginal number of effects. The decline of the MEE and MSFRV productions enjoined the reduction of the recovery ratio from 52% to 16%. Nevertheless, at the highest *dTc*, less energy was utilized by the MSFRV but rendered greater energy consumption by the B1 booster. Indeed, the vapor production of B1

Table 3. Exergy analysis of the proposed configurations

Stream	MSFRV				MSF-HYB				MSF-BHYB			
	m (kg/s)	T (C)	x (ppm)	E (kW)	m (kg/s)	T (C)	x (ppm)	E (kW	m (kg/s)	T (C)	x (ppm)	E (kW)
1	5,920	25	35,000	14,586	5,920	25	35,000	14,586	16,059	25	35,000	39,568
2	6,068	25	0	0	6,068	25	0	0	--	--	--	--
3	5,516	74.8	37,561	102,914	4,066	49	53,235	39,087	3,261	51	59,760	38,702
4	404	59.8	0	3,176	404	60	0	3,176	418	59	0	3,155
5	6,068	35	0	4,165	6,068	35	0	4,165	9,491	38	35,000	35,555
6	--	--	--	--	1,451	50	0	6,152	2,536	48	0	9,217
7	--	--	--	--	--	--	--	--	246	36	64,260	2,152
8	--	--	--	--	--	--	--	--	107	28	64,182	827
$Q^{\#}$ (kW)	204,246				111,407				155,969			
dE (kW)	108,576				73,412				105,929			
Eff	0.496				0.583				0.542			

$$Q\# = Q\left(1 - \frac{T_o}{T}\right)$$

raised but it was countered by reduction in B2 booster as T_{hi} decreased. In addition, the vapor produced by B1 has no boosting role as mentioned earlier. Moreover, the amount of vapor produced by B1 was much smaller than that of the primary MEE.

3-7. Exergy analysis

An additional way to compare these proposed configurations was via exergy analysis. The exergy destruction and exergy efficiency of MSFRV, HYB, and BHYB configurations were evaluated using Eqs. (30-34). The exergy equations were applied to the flow streams highlighted by red numbers in Fig. 1a (MSFRV), Fig. 2 (HYB), and Fig. 3 (BHYB). Note for each configuration, the waste heat input (Q) was included in the exergy calculations as reversible work. Q was computed as the sensible heat required to raise the temperature of the main feed to T_f. Since T_f was fixed for all structures, Q would vary for each structure because of the difference in inlet temperature, i.e., T_{fo} for MSFRV, and T_{f1} for HYB and BHYB systems. Note that T_{f1} also differed between HYB and BHYB systems/The temperature of the waste energy source was assumed to be at $T_f + 5$ ℃.

The result was listed in Table 3. Clearly, the standalone MSFRV was the least efficient system for having the highest exergy losses and least exergy efficiency. Indeed, hybridization not only improved distillate production but also reduced entropy production and improved the exergy efficiency. The boosted hybrid system seemed to be inferior to the hybrid system in terms of exhibiting 44% larger exergy losses and slightly less exergy efficiency which amounts to 7%. The inferiority of BHYB relative to the HYB system can be attributed to the following reasons. First, the amount of waste heat used by the BHYB system was greater because of the difference in T_{f1}, the seawater temperature before being heated by the waste heat source. In fact, T_{f1} was 38 ℃ and 50 ℃ for the BHYB and HYB systems, respectively. The second reason was that the BHYB system acquired a higher amount of seawater intake to condense the augmented vapor production at the down condenser. Note that the BHYB system generated an escalated quantity of vapor due to the incorporation of boosters. Moreover, the access amount of seawater intake was rejected at higher temperature increasing entropy generation. Although the BHYB had better energy utilization to generate additional distillate, the augmented heat input and seawater intake generated additional irreversibility compared to the HYB system. Hence, the BHYB system needed design or operation condition modification to make it more efficient. For example, the rejected seawater could be used to power another booster unit or mixed with the MEE feed. Another way was to utilize the MEE reject brine, which was at a relatively high temperature, to power additional booster units. For better visualization of the exergy analysis of the three systems, an exergy flow diagram was shown in Fig. 10. Clearly, the magnitude of exergy destruction depended heavily on the total exergy flow to the system. For example, MSFRV had the largest input exergy because it incurred the highest energy supply by the waste energy source. Thus, it rendered the worst exergy losses. On the other hand, the HYB structure had the least input

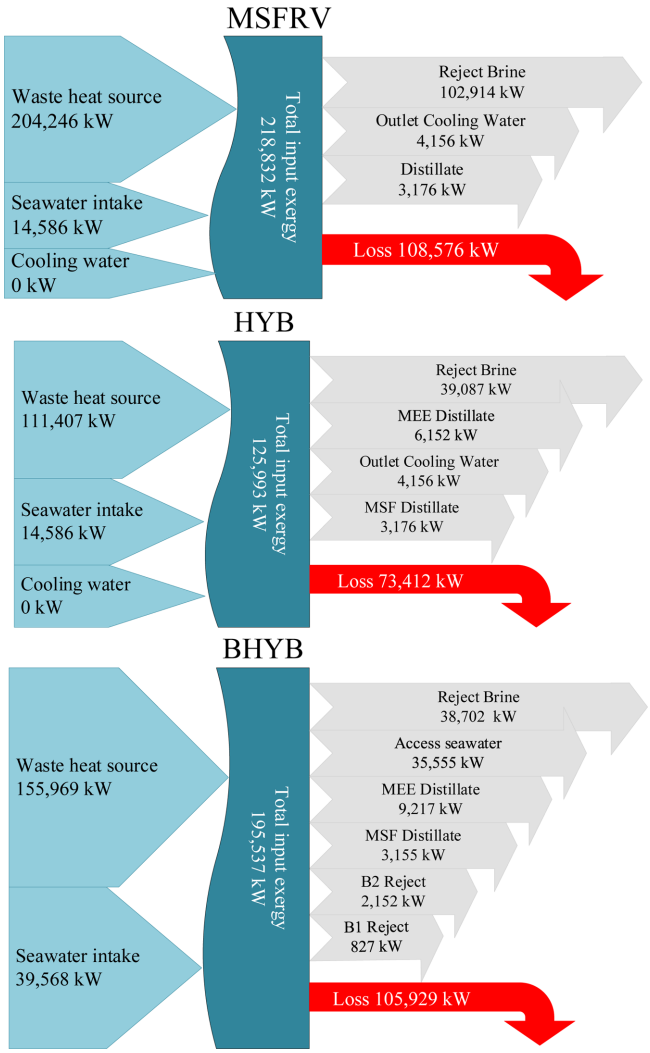

Fig. 10. Exergy Flow Diagram of MSFRV, HYB, and BHYB systems.

exergy as it used the least energy demand from the waste energy source. Therefore, it engendered the least exergy losses. Accordingly, the most efficient structure was the one that is being designed to use minimum external energy. Moreover, the MSFRV's exergy flow indicated that the MSF brine carrier large useful work. By utilization of this work via hybridization, the entropy of the brine was reduced to 39,087 kW in the HYB system and to 38,702 kW in the BHYB system. Furthermore, the BHYB's exergy flow showed high entropy was associated with access seawater which should be optimally utilized.

4. Conclusions

Integration of MEE and MSFRV systems to be powered by a waste heat source was presented and studied. The essence of integration was to harness the thermal energy inherited with the MSFRV reject brine. The recovered thermal energy should serve as a sensible heat supply to the MEE system. Two hybrid structures denoted as HYB and BHYB were proposed and compared. Both hybrid structures delivered enhanced performance over the standalone MSFRV. Based on the best hybrid structure (BHYB), the recovery ratio, the specific

energy consumption, and GOR can reach 561%, 91%, and 83%, improvement, respectively over the standard MSFRV process. The hybrid structure that incorporated booster units (BHYB) outperformed the other structure. The supplementary boosters provided additional vapor production, hence improving the overall production and consequently the other related performance indicators such as the specific area, the specific energy consumption, and GOR. The boosters efficiently leveraged the internal energy to produce additional distillate and avoid using additional heat exchangers and external cooling water. The parametric analysis illustrated the positive effect of the primary feed temperature, the temperature drop of the MEE sensible heat supplier, and the differential effect's temperature on the overall performance. For example, using a primary feed temperature of 85 ℃ and a temperature drop of 15 ℃ across the MEE's heat supplier can improve the recovery ratio and GOR of BHYB up to 65% and 25%, compared to that of the HYB structure. It was also found that it was better to use the smallest temperature drop per effect to maximize the number of effects such that the supplied energy was efficiently harnessed. It was also recommended to make the number of effects adaptive with the primary feed temperature and the temperature drop of the sensible heat as they have opposite effect on the top brine temperature. The exergy analysis indicated that the HYB structure was the most efficient as it has the least exergy losses of 73,412 kW and the highest exergy efficiency of 58%. This was due to better distribution of the thermal energy within the system and lesser irreversibility sources. It should be noted that performance enhancement due to hybridization had an impact on plant economics. Hybridization incurred additional equipment such as pumps, heat exchangers, etc, which would increase the capital and operation costs. Hence economic analysis was necessary to assess the tradeoff between efficiency and production cost.

Acknowledgment

This project is funded by the Ongoing Research Funding Program (ORF-2025-510), King Saud University, Riyadh, Saudi Arabia.

Conflict of Interest

The authors declare that they have no known competing financial interests or personal relationships that could have appeared to influence the work reported in this paper

Nomenclature

A_c : MSF Condenser tube surface area [m^2]
A_{dc} : MEE down condenser surface area [m^2]
A_{bc} : MSF Brine cooler surface area [m^2]
A_{bh} : Heat exchanger (HE01) surface area [m^2]
A : MEE evaporator surface area [m^2]
B : Brie flow rate in MEE [kg/s]
BPR : Boiling point elevation [℃]
C_p : Heat capacity [kJ/kg.K]
D : MEE distillate flow rate [kg/s]
D_{MSF} : Total MSF distillate flow rate [kg/s]
D_{MEE} : Total MEE distillate flow rate [kg/s]
D_t : Total MSF + MEE distillate flow rate [kg/s]
DTC : Cross temperature drop [C]
dTc : Temperature drop at MSF brine cooler and C2 [C]
dTb : Design parameter [C]
dTh : Temperature drop for the MEE heat supply [C]
dT_{cw} : Temperature drop at MSF brine cooler C1 in case of S3 structure [C]
F : MEE feed flow rate for each effect [kg/s]
F_{B1}, F_{B2}: Feed flow rate for booster 1 and booster 2 [kg/s]
GOR : Gain output ratio
h : Enthalpy [kJ/kg]
h_{fg} : Latent heat [kJ/kg]
h_d : Enthalpy of the distillate [kJ/kg]
h_c : Enthalpy of the condenser stream [kJ/kg]
j : Stage number
$LMTD$: Logarithmic mean temperature difference
m_f : Seawater feed flow rate [kg/s]
m_b : MSF Brie stream flow rate [kg/s]
m_{b_n} : Brine flow rate exiting MSF [kg/s]
m_d : MSF Distillate flow rate [kg/s]
m_{cw} : Coolant mass rate [kg/s]
m_s : Flow rate of heating fluid for MEE [kg/s]
n : Number of MSF stages
ne : Number of MEE effects
PR : Performance ratio
Q_a : Available sensible heat [kJ/s]
Q_{cool} : Cooling rate [kJ/s]
Q_{heat} : Heating rate [kJ/s]
R_{cw} : Coolant water ratio
RR : Recovery ratio
RV : Reversal
S : Salinity [kg/m^3]
SEC : Specific energy consumption [kWh/m^3]
sA : Specific area [m^2/(kg/s)]
sCw : Specific cooling water [-]
T : MSF Condenser temperature [℃]
T_b : Brine Temperature [℃]
T_d : Distillate temperature [℃]
T_f : MSF Feed Temperature [℃]
T_{fo} : Fresh feed temperature [℃]
T_{ff} : MEE feed temperature [℃]
T_v : Vapor temperature [℃]
T_{hi} : Inlet temperature to MEE heat supplier [℃]
T_{ho} : Outlet temperature of MEE heat supplier [℃]
T_n : Brine temperature leaving brine cooler [℃]
T_{bn} : Brine temperature exiting stage n [℃]

T_{c1} : Coolant inlet temperature [℃]
T_{c2} : Coolant outlet temperature [℃]
T_1 : MSF Condenser stream temperature exiting stage 1 [℃]
T_{cw} : Seawater intake temperature [℃]
U_{bh} : Heat transfer coefficient for HE01 [kW/m^2.℃]
U : Heat transfer coefficient for MEE evaporator [kW/m^2.℃]
U_{bc} : Heat transfer coefficient for MSF brine cooler [kW/m^2.℃]
U_c : Heat transfer coefficient for MSF condenser tube [kW/m^2.℃]
U_{dc} : Heat transfer coefficient for MEE down condenser tube [kW/m^2.℃]
V : MEE vapor flow rate [kg/s]
x_f : Seawater feed salinity [ppm]
x_b : Brine stream salinity [ppm]
x_{bn} : Salinity of the brine exiting stage n [ppm]
x_1 : Salinity of MSF brine exiting stage 1 [ppm]
x : Salinity [ppm]

References

1. Ahmad, N. A., Goh, P. S., Yogarathinam, L. T., Zulhairun, A. K. and Ismail, A. F., "Current Advances in Membrane Technologies for Produced Water Desalination," *Desalination*, **493**, 114643 (2020).
2. Pointet, T., "The United Nations World Water Development Report 2022 on Groundwater, a Synthesis," *LHB*, **108**(1), 2090867 (2022).
3. Economic, U.N.D.o.I., World population prospects. 1978: UN.
4. Rahimi, B., Christ, A., Klaus, R. and Hui, T. C., "A Novel Process for Low Grade Heat Driven Desalination," *Desalination*, **351**, 202-212(2014).
5. Hesari, F., Salimnezhat, F., Manesh, M. H. K. and Morad, M. R., "A Novel Configuration for Low-grade Heat-driven Desalination Based on Cascade MED," *Energy*, **229**, 120657(2021).
6. Dastgerdi, H. R., Whittaker, P. B. and Chua, H. T., "New MED Based Desalination Process for Low Grade Waste Heat," *Desalination*, **395**, 57-71(2016).
7. Camacho, L. M., Ludovic, D., Jianhau, Z., Li, J., Mikel, D., Gomez, J. and Gray, S., "Advances in Membrane Distillation for Water Desalination and Purification Applications," *Water*, **5**(1), 94-196(2013).
8. Ghaffour, N., Missimer, T. M. and Amy, G. L., "Technical Review and Evaluation of the Economics of Water Desalination: Current and Future Challenges for Better Water Supply Sustainability," *Desalination*, **309**, 197-207(2013).
9. Gude, V. G., "Energy Storage for Desalination Processes Powered by Renewable Energy and Waste Heat Sources," *Applied Energy*, **137**, 877-898(2015).
10. Eke, J., Yusuf, A., Giwa A. and Sodiq, A., "The Global Status of Desalination: An Assessment of Current Desalination Technologies, Plants and Capacity," *Desalination*, **495**, 114633(2020).
11. Goosen, M. F., Mahmoudi, H. and Ghaffour, N., "Today's and Future Challenges in Applications of Renewable Energy Technologies for Desalination," *Critical Reviews in Environmental Science and Technology*, **44**(9), 929-999(2014).
12. Abdelkareem, M. A., Assad, M. E. H., Sayed, E. T. and Soudan, B., "Recent Progress in the Use of Renewable Energy Sources to Power Water Desalination Plants," *Desalination*, **435**, 97-113(2018).
13. Alkaisi, A., Mossad, R. and Sharifian-Barforoush, A., "A Review of the Water Desalination Systems Integrated with Renewable Energy," *Energy Procedia*, **110**, 268-274(2017).
14. Mathioulakis, E., Belessiotis, V. and Delyannis, E., "Desalination by Using Alternative Energy: Review and State-of-the-art," *Desalination*, **203**(1-3), 346-365(2007).
15. Capocelli, M., Moliterni, E., Piemonte, V. and De Falco, M., "Reuse of Waste Geothermal Brine: Process, Thermodynamic and Economic Analysis," *Water*, **12**(2), 316(2020).
16. Barba, D. and Capocelli, M., "Process Analysis of the Novel Flash-ME Desalination Process Driven by Low-grade Thermal Energy," *Chemical Engineering Research and Design*, **189**, 721-733(2023).
17. Papapetrou, M., Kosmadakis, G., Cipollina, A., La commare, U. and Micale, G., "Industrial Waste Heat: Estimation of the Technically Available Resource in the EU Per Industrial Sector, Temperature Level and Country," *Applied Thermal Engineering*, **138**, 207-216 (2018).
18. Hernández, J., Romero, R. J., Juarez, D., Escobar, R. F. and Siqueiros, J., "A Neural Network Approach and Thermodynamic Model of Waste Energy Recovery in a Heat Transformer in a Water Purification Process," *Desalination*, **243**(1-3), 273-285(2009).
19. Datsgerdi, H. R. and Chua, H. T., "Thermo-economic Analysis of Low-grade Heat Driven Multi-effect Distillation Based Desalination Processes," *Desalination*, **448**, 36-48(2018).
20. Christ, A., Regenauer-Lieb, K. and Chua, H. T., "Thermodynamic Optimisation of Multi Effect Distillation Driven by Sensible Heat Sources," *Desalination*, **336**, 160-167(2014).
21. Helal, A., Hybridization—a New Trend in Desalination," *Desalination and Water Treatment*, **3**(1-3), 120-135(2009).
22. Hamed, O. A., "Overview of Hybrid Desalination Systems—current Status and Future Prospects," *Desalination*, **186**(1-3), 207-214(2005).
23. Ghaffour, N., Soukane, S., Lee, J. G., Kim, Y. and Alpatova, A., "Membrane Distillation Hybrids for Water Production and Energy Efficiency Enhancement: A Critical Review," *Applied Energy*, **254**, 113698(2019).
24. Dahdah, T. H. and Mitsos, A., "Structural Optimization of Seawater Desalination: II Novel MED–MSF–TVC Configurations," *Desalination*, **344**, 219-227(2014).
25. Zak, G. M. and Mitsos, A., "Hybrid Thermal–thermal Desalination Structures," *Desalination and Water Treatment*, **52**(16-18), 2905-2919(2014).
26. Al-Mutaz, I. S. and Wazeer, I., "Current Status and Future Directions of MED-TVC Desalination Technology," *Desalination and Water Treatment*, **55**(1-3), 1-9(2015).
27. Ihm, S., Alnajdi, O. Y., Hamid, O. A., Jun, G. and Chung, H., "Energy Cost Comparison Between MSF, MED and SWRO: Case Studies for Dual Purpose Plants," *Desalination*, **397**, 116-125(2016).
28. Tufa, R. A., Curcio, E., Brauns, E., Van Baak, W., Fontananova, E. and Di Profio, G., "Membrane Distillation and Reverse Electrodialysis for Near-zero Liquid Discharge and Low Energy Seawater Desalination," *Journal of Membrane Science*, **496**, 325-333(2015).
29. Farsi, A. and Dincer, I., "Development and Evaluation of An Integrated MED/membrane Desalination System," *Desalination*, **463**, 55-68(2019).
30. Aly, S., Jawad, J., Manzoor, H., Simson, S., Lawler, J. and Mabrouk,

A. N., "Pilot testing of a novel integrated Multi Effect Distillation-Absorber Compressor (MED-AB) Technology for High Performance Seawater Desalination," *Desalination*, **521**, 115388(2022).
31. Baig, H., Antar, M. A. and Zubair, S. M., "Performance Evaluation of a Once-through Multi-stage Flash Distillation System: Impact of Brine Heater Fouling," *Energy Conversion and Management*, **52**(2), 1414-1425(2011).
32. Ali, E., Orfi, J., Alansary, H., Alsaadi, A. S. and Ghafour, N., "Novel Multistage Flash Reversal Concept: Modelling and Analysis," *Applied Thermal Engineering*, **217**, 119223(2022).
33. Ali, E., Orfi, J., Alansary, H., Baakeem, A., Alsaadi, A. S. and Ghaffour, N., "Concept and Analysis of Hybrid Reversal Multi-stage Flash and Membrane Distillation Desalination System," *Environmental Technology*, **45**(24), 5218-5231(2023).
34. Ali, E., Orfi, J., Alansary, H., Baakeem, A., Alsaadi, A. S. and Ghaffour, N., "Advanced Structures of Reversal Multi-stage Flash Desalination," *Desalination*, **571**, 117095(2024).
35. Ali, E., Orfi, J., Alsaadi, A. S., Ghaffour, N. and Khennich, M., "Improved Modelling and Simulation of Once-through and Reverse Multi-stage Flash Desalination Configurations," *The Canadian Journal of Chemical Engineering*, **101**, 7173-7190(2023).
36. Roy, Y., Thiel, G. P. and Antar, M. A., "The Effect of Increased Top Brine Temperature on the Performance and Design of OT-MSF Using a Case Study," *Desalination*, **412**, 32-38(2017).
37. El-Dessouky, H. T. and Ettouney, H. M., Fundamentals of Salt Water Desalination, Elsevier, Amsterdam, Netherland(2002).
38. Darwish, M. and Abdulrahim, H. K., "Feed Water Arrangements in a Multi-effect Desalting System," *Desalination*, **228**(1-3), 30-54(2008).
39. Zhou, S., Shen, S., Guo, Y. and Mu, X., "Comparative Performance Evaluation of LT-MEE Desalination Systems with Three Feed Configurations," *Desalination and Water Treatment*, **269**, 217-228(2017).
40. Al-Mutaz, I. S. and Wazeer, I., "Development of a Steady-state Mathematical Model for MEE-TVC Desalination Plants," *Desalination*, **351**, 9-18(2014).
41. Ali, E., Orfi, J., Alansary, H., Lee, J. G., Alpatova, A. and Ghaffour, N., "Integration of Multi Effect Evaporation and Membrane Distillation Desalination Processes for Enhanced Performance and Recovery Ratios," *Desalination*, **493**, 114619(2020).
42. Rahimi, B., Marvi, Z., Alamolhoda, A. A., Abbaspour, M. and Chua, H. T., "An Industrial Application of Low-grade Sensible Waste Heat Driven Seawater Desalination: A Case Study," *Desalination*, **470**, 114055(2019).
43. Nayar, K. G., Sharqawy, M. H. and Banchik, L. D., "Thermophysical Properties of Seawater: A Review and New Correlations That Include Pressure Dependence," *Desalination*, **390**, 1-24(2016).
44. Sharqawy, M. H., Lienhard, J. H. and Zubair, S. M., "Thermophysical Properties of Seawater: A Review of Existing Correlations and Data," *Desalination and Water Treatment*, **16**(1-3), 354-380(2010).
45. Rahimi, B., May, J., Christ, A., Regenauer-Lieb, K. and Chua, H. T., "Thermo-economic Analysis of Two Novel Low Grade Sensible Heat Driven Desalination Processes," *Desalination*, **365**, 316-328(2015).

Authors

Emad Ali: Professor, Chemical Engineering Department, King Saud University, Riyadh, 11421, Saudi Arabia; amkamal@ksu.edu.sa

Jamel Orfi: Professor, Mechanical Engineering Department, King Saud University, Riyadh, 11421, Saudi Arabia; orfij@ksu.edu.sa

Appendix A: Supporting Correlations

Heat capacity	$C_p\left(\frac{J}{kg\cdot K}\right) = a + bT + cT^2 + dT^3$	(A.1)
	$a = 4206.8 - 6.6197 \times S + 1.2288 \times 10^{-2} \times S^2$ $b = -1.1262 + 5.4178 \times 10^{-2} \times S - 2.2719 \times 10^{-4} \times S^2$ $c = 1.2026 \times 10^{-2} - 5.3566 \times 10^{-4} \times S + 1.8906 \times 10^{-6} \times S^2$ $d = 6.8777 \times 10^{-7} + 1.517 \times 10^{-6} \times S - 4.4268 \times 10^{-9} \times S^2$ $S = x/1000$	(A.2)
Latent heat	h_{fg} (kJ/kg) = 2589.583 + 0.9156 × T (°C) − 4.834 × 10^{-2} × T^2(°C)	(A.3)
Heat Transfer coefficient	U (kw/m^2·C) = 1.7194 + 3.2063 × 10^{-3} × T (°C) + 1.5971 × 10^{-5} × T^2(°C) − 1.9918 × 10^{-7} × T^3(°C)	(A.4)
Boiling point rise	BPR = (0.0143 x + 2.423 × 10^{-7} x^2) × 10^{-3}	(A.5)
Key performance index		
sA	$\frac{A_{dc} + A_{bc} + A_{bh} + \sum A_i + \sum A_{c,i}}{D_t}$	(A.6)
GOR	$\frac{\sum m_{d_i} h_{fg}(T_{vi}) + \sum D_i h_{fg}(T_{di})}{Q_{heat}}$	(A.7)
SEC	$\frac{Q_{cool} + Q_{heat}}{D_t}$	(A.8)
RR	$\frac{D_t}{m_f} \times 100$	(A.9)
PR[6]	$D_t \times 2336/Q_a$	(A.10)
sC_w	$sC_w = m_{cw}/D_t$	(A.11)

Appendix B: Simulation Organigram

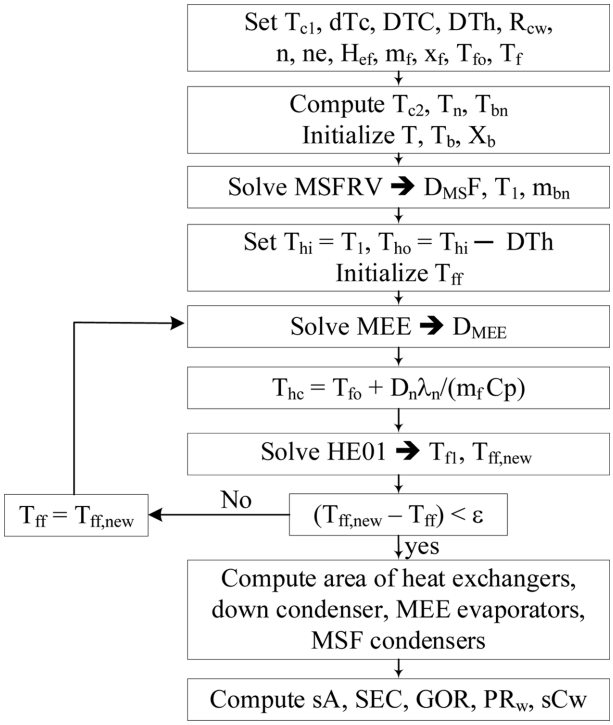

Fig. B1. Organigram for the numerical solution of the hybrid system HYB

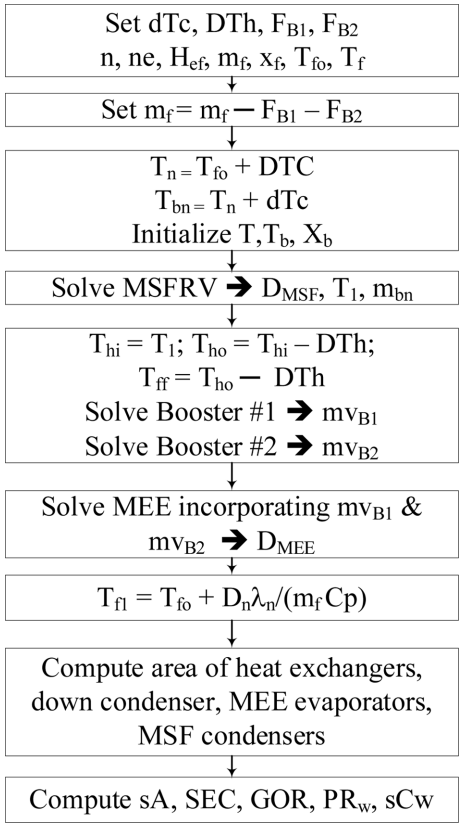

Fig. B2. Organigram for the numerical solution of the hybrid system BHYB